HAL
archives-ouvertes.fr

Attenuated internal reflection terahertz imaging

Antoine Wojdyla, Guilhem Gallot

▶ **To cite this version:**

Antoine Wojdyla, Guilhem Gallot. Attenuated internal reflection terahertz imaging. Optics Letters, Optical Society of America, 2013, 38 (2), pp.112-114. hal-00817162

HAL Id: hal-00817162

https://hal-polytechnique.archives-ouvertes.fr/hal-00817162

Submitted on 25 Feb 2014

HAL is a multi-disciplinary open access archive for the deposit and dissemination of scientific research documents, whether they are published or not. The documents may come from teaching and research institutions in France or abroad, or from public or private research centers.

L'archive ouverte pluridisciplinaire **HAL**, est destinée au dépôt et à la diffusion de documents scientifiques de niveau recherche, publiés ou non, émanant des établissements d'enseignement et de recherche français ou étrangers, des laboratoires publics ou privés.

Attenuated internal reflection terahertz imaging

Antoine Wojdyla[1,2] and Guilhem Gallot[1,2,*]

[1]*Laboratoire d'Optique et Biosciences, École Polytechnique, CNRS, 91128 Palaiseau, France*

[2]*INSERM U696, 91128 Palaiseau, France*

Corresponding author: guilhem.gallot@polytechnique.edu

Received November 22, 2012; accepted November 30, 2012;
posted December 4, 2012 (Doc. ID 180312); published January 7, 2013

We present a terahertz (THz) imaging technique based on attenuated internal reflection, which is ideally suited for the analysis of liquid and biological samples. Inserted in a THz time-domain system, and using a high-resistivity low loss silicon prism to couple the THz wave into the sample, the detection scheme is based on the relative differential spectral phase of two orthogonal polarizations. Biological sample imaging as well as subwavelength ($\lambda/16$) longitudinal resolution are demonstrated. © 2013 Optical Society of America

OCIS codes: 170.6795, 110.5405, 170.3880.

The terahertz (THz) band of the electromagnetic spectrum experienced major breakthroughs during the past two decades. Among other techniques, time-resolved imaging has been proven to be a convenient tool to provide contrast in the study of objects, to bring together good resolution of optics, and to show the capabilities of microwave penetration. Most of them are based on transmission or reflection and sometimes use near-field techniques to enhance the resolution for either raster-scan or direct imaging [1–6]. When it comes to analyzing aqueous samples, the main drawback is most of the energy is lost due to either high-absorption in transmission techniques (≈300 cm^{-1} at 1 THz for water [7]) or low partial external reflection coefficient (≈30%) [8]. In addition, these techniques often require reference measurements and perfectly controlled surfaces, conditions that could be difficult to gather when it comes to studying biological samples. Furthermore, resolution is typically limited by diffraction to a few hundred micrometers.

We present here the development of attenuated total reflection (ATR) for imaging purpose in the THz domain. ATR is a well-known technique in visible and infrared domain [9,10]. Extending to the THz domain, attenuated internal reflection THz imaging (AIRTI) relies on the phase shift that occurs at total internal reflection at the interface between two media. This technique is based on the evanescent wave created at the ATR interface, which has a very limited longitudinal extension. Thus, the interaction length of the wave is reduced, which is particularly valuable when the sample under examination is highly absorptive in the THz range, like polar liquids and aqueous samples. AIRTI will exhibit diffraction limited lateral and subwavelength longitudinal resolution, high-sensitivity, and suitability with biological samples.

Total internal reflection occurs when light impinges on a dielectric interface for which the inner medium has a larger refraction index n_1 than the outer medium index n_2, and when the angle of incidence α is over the critical angle α_c, defined by $\alpha_c = \arcsin|n_2/n_1|$. Under these conditions, the reflection coefficient is unitary and complex: the reflection has a phase-shift which depends on the polarization component. At the interface in the outer medium, an evanescent wave takes place, characterized by an imaginary wave-vector and an exponential decay $\exp(-L/d)$, with

$$d = \frac{c}{2\pi\nu\sqrt{n_1^2 \sin^2\alpha - n_2^2}}, \tag{1}$$

where ν is the frequency [11]. For absorptive medium, total internal reflection is actually an ATR that has been widely used to perform spectroscopic measurement on highly absorbing medium, water for instance [12]. Reflection is no more total, and amplitude and dephasing strongly depends on the outer medium complex dielectric constant. Azzam showed that the most sensitive incidence angle area lies between critical angle α_c and Brewster's angle $\alpha_B = \arctan|n_2/n_1|$ [13]; for pure water, $\varepsilon \approx 4.28 + i3.16$ at 1 THz [7], and then $\alpha_B \approx 34°$ and $\alpha_c \approx 43°$.

To provide an internal reflection condition, we use a very transparent high-resistivity silicon (HR-Si) isosceles prism ($R > 10$ kΩ · cm, $n = 3.42$ [14]) with a base angle of $\alpha = 42°$, which fulfills Azzam's condition and furthermore provides a $\pi/2$ phase shift in air between s- and p-polarization components. This incident angle enables AIRTI condition for external medium refractive index up to $n_{\text{ext}} = 2.27$ and is therefore compatible with liquid water. To ensure imaging capabilities, the silicon prism is topped with a 3 mm HR-Si patch on which the samples are placed and which can be mechanically moved (Fig. 1).

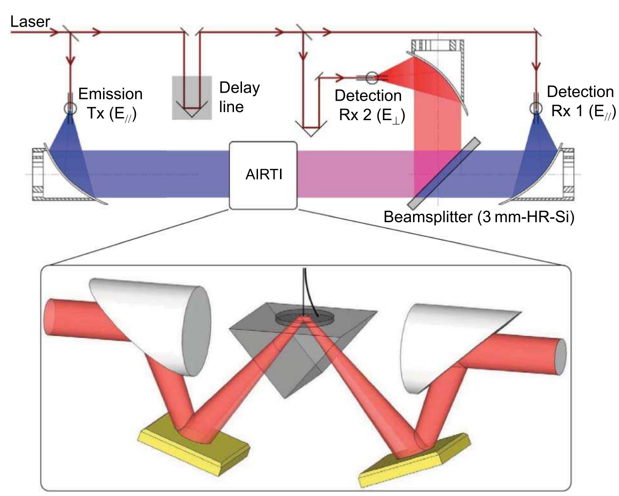

Fig. 1. (Color online) Experimental THz-TDS setup with complete polarization characterization (top), including AIRTI system (bottom).

0146-9592/13/020112-03$15.00/0 © 2013 Optical Society of America

The THz beam is focused outside the prism by an off-axis parabolic mirror (PM, NA $= 0.16$) tuned so that the focal point is located at the internal reflection interface. It should be noted that plenty of space is available above the prism to put biological samples and related controls.

The THz signal is generated by a classical THz time-domain spectroscopy (THz-TDS) setup [15], composed of a GaAs photoconductive transmitter (Tx) lit by a 12 fs 76 MHz Femtolaser titanium-sapphire laser that generates an almost linearly s-polarized subsingle cycle THz pulse, centered around 1 THz and extending to up to 4 THz (Fig. 1). In order to increase the detection sensitivity, we fully characterize the THz pulse, in amplitude, phase and polarization. For that purpose, the THz beam is collimated by a PM and polarized at 45° by a 4 silicon wafers Brewster's polarizer (P) [16], thus creating an equal mixture of in-phase s- and p-polarized waves. The beam is then split into two almost equal beams by a 3 mm thick 100 mm diameter high resistivity silicon wafer orientated at 45° ($t_p = 0.82$, $r_s = -0.65$ in amplitude). The HR-Si beam splitter is thick enough to avoid pulse echoes during measurements. Then, the two polarization components are independently focused by PMs and finally detected by two orthogonal LT-GaAs photoconductive receivers (Rx), each detecting only one component of the THz wave. A main delay line allows a scan of the waveform of the two polarization components, while the other allows fine tuning of the optical path between the two Rx.

Various types of scans can be performed. Complete pulse scan for each (X, Y) position provides more information. This kind of high-precision measurement can be performed in less than an hour (20×20 pixels with 200 μm step, 80 delay-line positions with 10 μm steps, 30 ms integration time with 24 dB/oct roll-off, three times zero padding). Other types of faster scans can be performed by setting constant delay line length, thus shortening the acquisition time (few minutes), and resulting in two-dimensional (X, Y) datasets.

To characterize AIRTI technique capabilities, we first imaged a cross engraved in an aluminum plate (500 μm-large, 1 mm-deep grooves), (Fig. 2, bottom, black solid lines). It is a pure phase object, for the beam experiences a metallic reflection when the beam bounces on aluminum or a total internal reflection when the beam bounces on air. The best contrast was obtained by measuring the differential spectral phase. Figure 2 (bottom) shows at 1 THz the differences between the two types of reflection: metallic and total internal reflection. As expected, the two components have a differential phase-shift of $\pi/2$. A measured cross-section (Fig. 2 top, red dots) is compared with the theory using a Gaussian focal point convolved with the groove section (Fig. 2 top, solid curve) with $\exp(-x^2/w^2)$ and $w = 1.22$ mm. This corresponds to about 20% above Rayleigh criterion $\Delta = 2.44\lambda f/n_1 \cdot \mathrm{NA}$. Since the focusing mirrors are outside the imaging prism, the numerical aperture is reduced by a factor n_1 by entering the prism. An equal factor then applies to Rayleigh criterion, which cancels out the benefit effect of the high-refractive index. The longitudinal resolution is assessed by the mean of evanescent wave two interface experiment [17]. We put a mirror on top of the HR-Si patch and gradually increase the spacing between the patch and the mirror using 12.5 μm spacers made of aluminum. Hence, the reflection condition gradually shifts from metallic to total internal reflection. Experimental data at 1 THZ are shown in Fig. 3 (dots), as well as calculations (black curve) and exponential fit (red curve) with $d = 19 \pm 2$ μm, corresponding to $\lambda/16$ and comparing well with Eq. (1). Note that d would increase in water to about 32 μm in the same geometry.

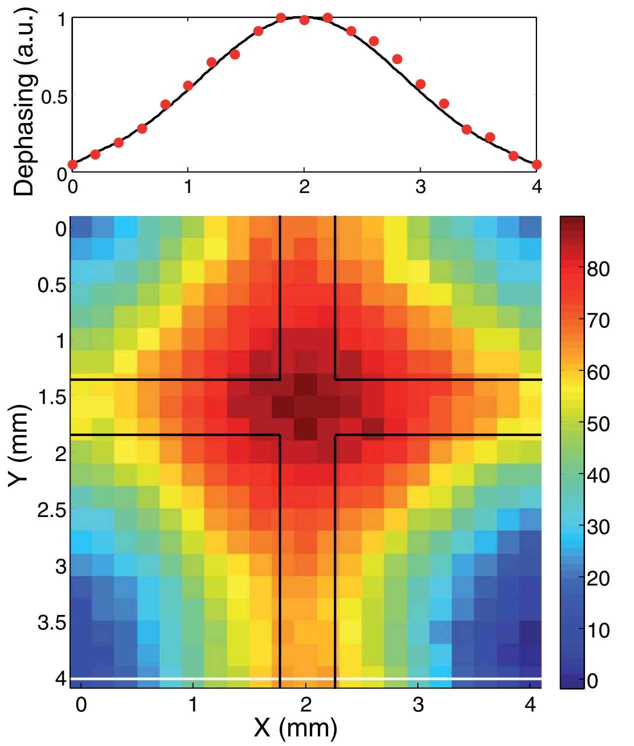

Fig. 2. (Color online) Differential spectral phase image at 1 THz of an aluminum cross (500 μm-large, 1 mm-deep, solid black lines). $\alpha = 42°$. Color bar unit is degree. Top graph is a cross-section (white horizontal line) with experimental data (dots) and Gaussian convolution fit (solid).

We then applied AIRTI to liquid water. Since pure water refractive index is less than the limit of 2.27 for an incidence angle of 42°, liquid water can be imaged using AIRTI, as can be shown in Fig. 4(a) in differential phase measurements, where a drop of distilled water is

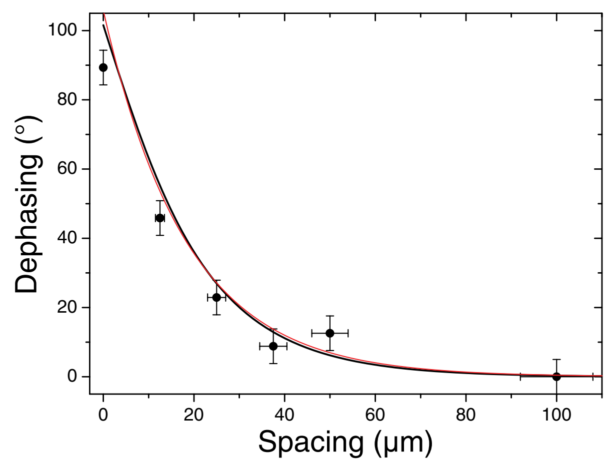

Fig. 3. (Color online) Dephasing of an aluminum plate versus spacing from AIRTI prism (dots), with theoretical calculation (black curve) and exponential fit (red curve) with $d = 19 \pm 2$ μm.

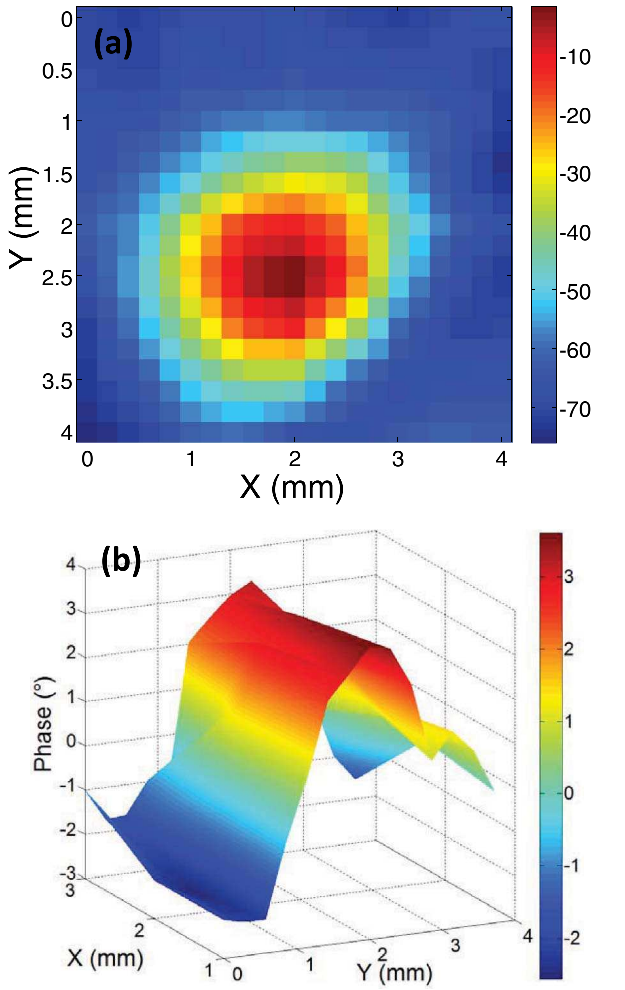

Fig. 4. (Color online) (a) Image of a water drop and (b) image of a frog sciatic axone. Color bars represent the differential phase in degree.

put on the mobile silicon patch. A strong dephasing of more than 80° can be observed. Since ions in liquid water slightly decreases the refractive index, conditions for imaging by AIRTI are even better [8]. A frog sciatic nerve of about 1 mm diameter bathed in a physiological solution is imaged in Fig. 4(b). The dephasing between the inner and the outer nerve is clearly observable and results in the ionic contrast in the nerve.

We demonstrated that attenuated internal reflection can be advantageously applied to THz imaging, in particular for biological samples. The detection scheme is based on the relative dephasing of two orthogonal polarizations, thus neither reference nor calibration are required. It shows good sensitivity, especially a sub-wavelength ability in longitudinal resolution, well suited for cell studies. The available space above the imaging prism is compatible with liquid water and biological sample requirements, and could be mixed with microfluidics. Transverse resolution could also be improved by increasing the numerical aperture at the interface using silicon lenses in contact with the prism.

The THz antennas have been realized at the technological platform of IEMN, cité scientifique, av. Poincaré BP 60069, 59652 Villeneuve d'Ascq, France.

References

1. B. B. Hu and M. C. Nuss, Opt. Lett. **20**, 1716 (1995).
2. W. L. Chan, J. A. Deibel, and D. Mittleman, Rep. Prog. Phys. **70**, 1325 (2007).
3. C. Jansen, S. Wietzke, O. Peters, M. Scheller, N. Vieweg, M. Salhi, N. Krumbholz, C. Jördens, T. Hochrein, and M. Koch, Appl. Opt. **49**, E48 (2010).
4. F. Blanchard, A. Doi, T. Tanaka, H. Hirori, H. Tanaka, Y. Kadoya, and K. Tanaka, Opt. Express **19**, 8277 (2011).
5. O. Mitrofanov, T. Tan, P. R. Mark, B. Bowden, and J. A. Harrington, Appl. Phys. Lett. **94**, 171104 (2009).
6. J. B. Masson and G. Gallot, Opt. Express **14**, 11566 (2006).
7. C. Ronne, P. O. Astrand, and S. R. Keiding, Phys. Rev. Lett. **82**, 2888 (1999).
8. J. B. Masson, M. P. Sauviat, J. L. Martin, and G. Gallot, Proc. Natl. Acad. Sci. USA **103**, 4808 (2006).
9. N. J. Harrick, *Internal Reflection Spectroscopy* (John Wiley & Sons, 1967).
10. D. Axelrod, T. P. Burghardt, and N. L. Thompson, Annu. Rev. Biophys. Bioeng. **13**, 247 (1984).
11. M. Born and E. Wolf, *Principles of Optics*, 6th ed. (Cambridge University, 1997).
12. H. Hirori, K. Yamashita, M. Nagai, and K. Tanaka, Jpn. J. Appl. Phys. **43**, 1287 (2004).
13. R. M. A. Azzam, J. Opt. Soc. Am. A **16**, 1700 (1999).
14. J. Dai, J. Zhang, W. Zhang, and D. Grischkowsky, J. Opt. Soc. Am. B **21**, 1379 (2004).
15. A. Podzorov and G. Gallot, Appl. Opt. **47**, 3254 (2008).
16. A. Wojdyla and G. Gallot, Opt. Express **19**, 14099 (2011).
17. H. Hirori, M. Nagai, and K. Tanaka, Opt. Express **13**, 10801 (2005).